†Electronic Supplementary Information (ESI) available.

‡ These authors contributed equally to this work.

# Supporting Information

## Electrochemically stable frustrated Lewis pairs on dual-metal hydroxide for electrocatalytic $CO_2$ reduction

Weining Zhang,‡[a,b,c] Yuandong Yan,‡[b] Jing Wang,‡[d] Zhenhua Yang,[b] Taozhu Li,[b] Hu Li,[b] Shicheng Yan,[b*] Tao Yu[a], Weiliu Fan[d] and Zhigang Zou[a,b]

[a] Collaborative Innovation Center of Advanced Microstructures, Jiangsu Key Laboratory for Nano Technology, National Laboratory of Solid State Microstructures, School of Physics, Nanjing University, No. 22 Hankou Road, Nanjing, Jiangsu 210093, P. R. China

[b] Eco-materials and Renewable Energy Research Center (ERERC), College of Engineering and Applied Sciences, Nanjing University, No. 22 Hankou Road, Nanjing, Jiangsu 210093, P. R. China

E-mail: yscfei@nju.edu.cn

[c] School of Physics and Physical Engineering, Qufu Normal University, Qufu 273165, P. R. China

[d] School of Chemistry and Chemical Engineering, Shandong University, Jinan 250100, P. R. China

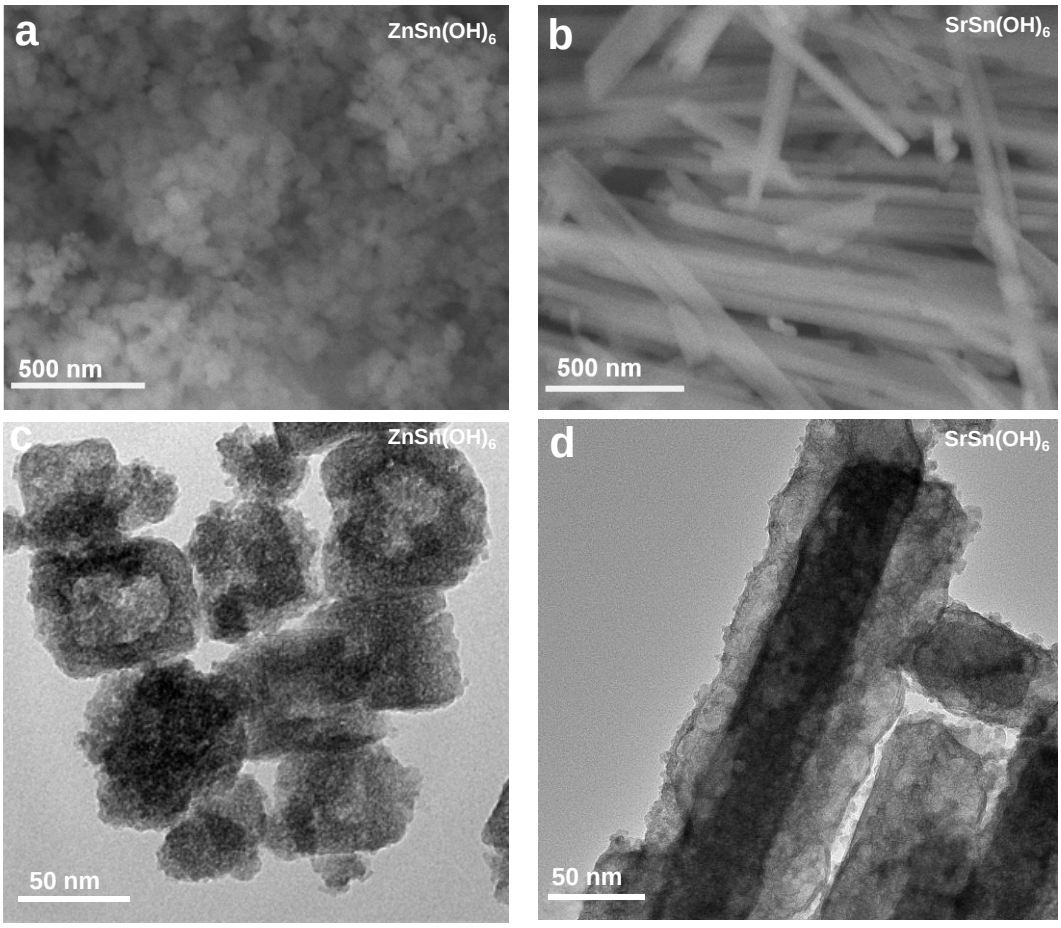


**Fig. S1.** The SEM and TEM images for as-prepared $ZnSn(OH)_6$ and $SrSn(OH)_6$ samples.

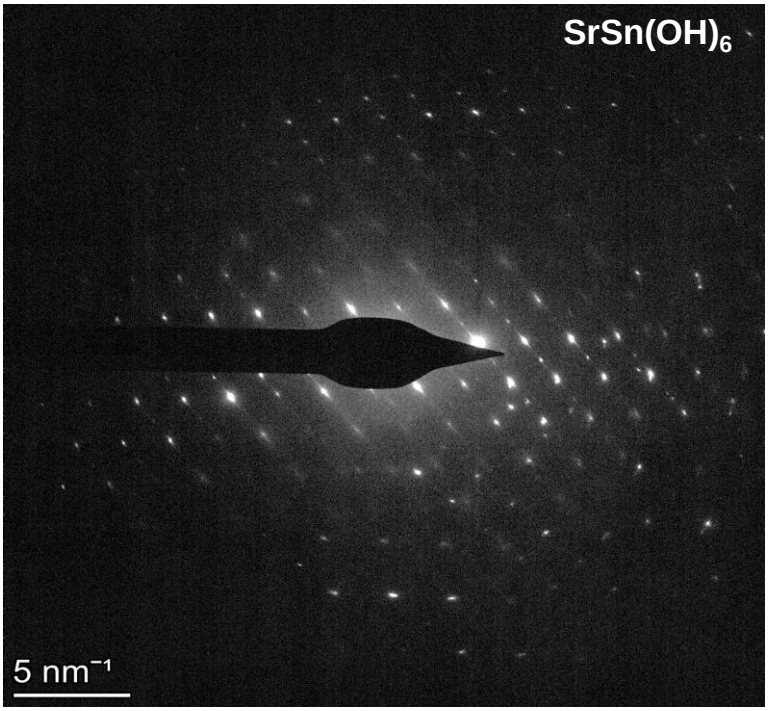


**Fig. S2.** The selected-area electron diffraction (SAED) image of $SrSn(OH)_6$.

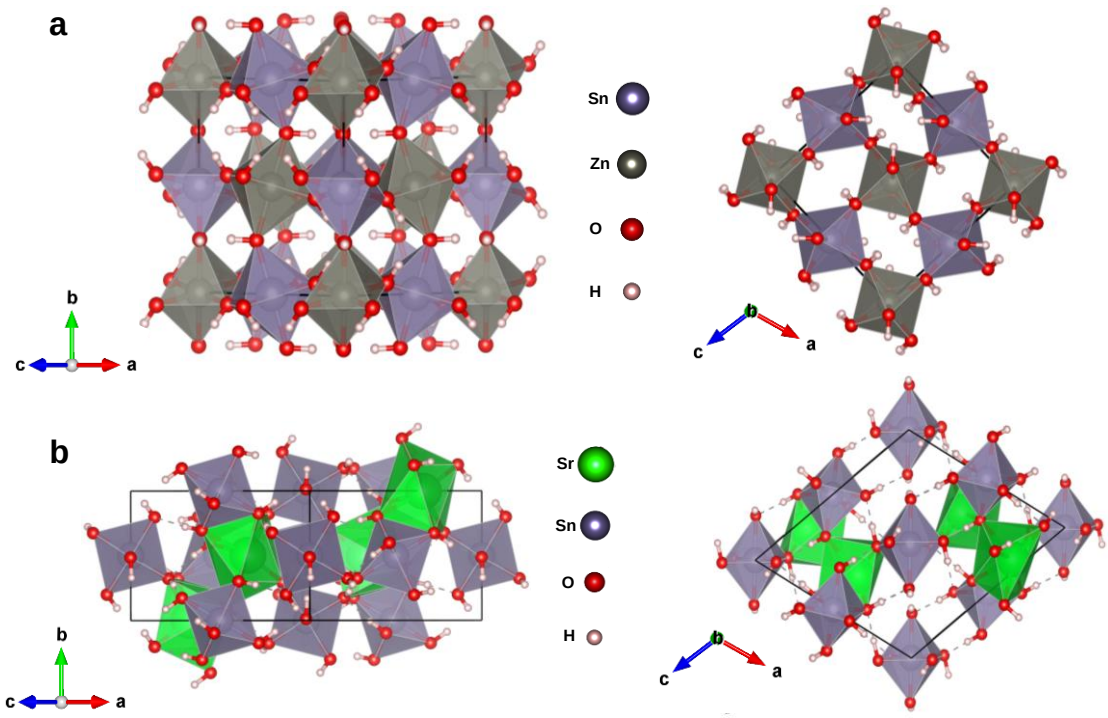


**Fig. S3.** The optimized cell structures for $ZnSn(OH)_6$ (a) and $SrSn(OH)_6$ (b).

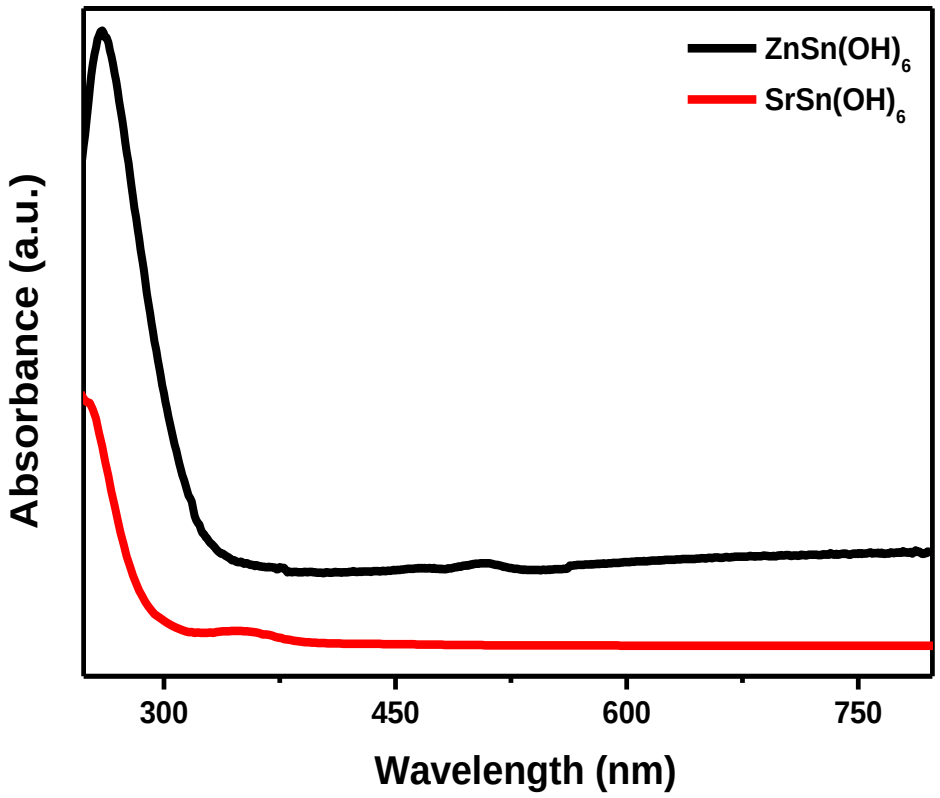


**Fig. S4.** The UV–Vis absorption spectra for $ZnSn(OH)_6$ and $SrSn(OH)_6$ samples.

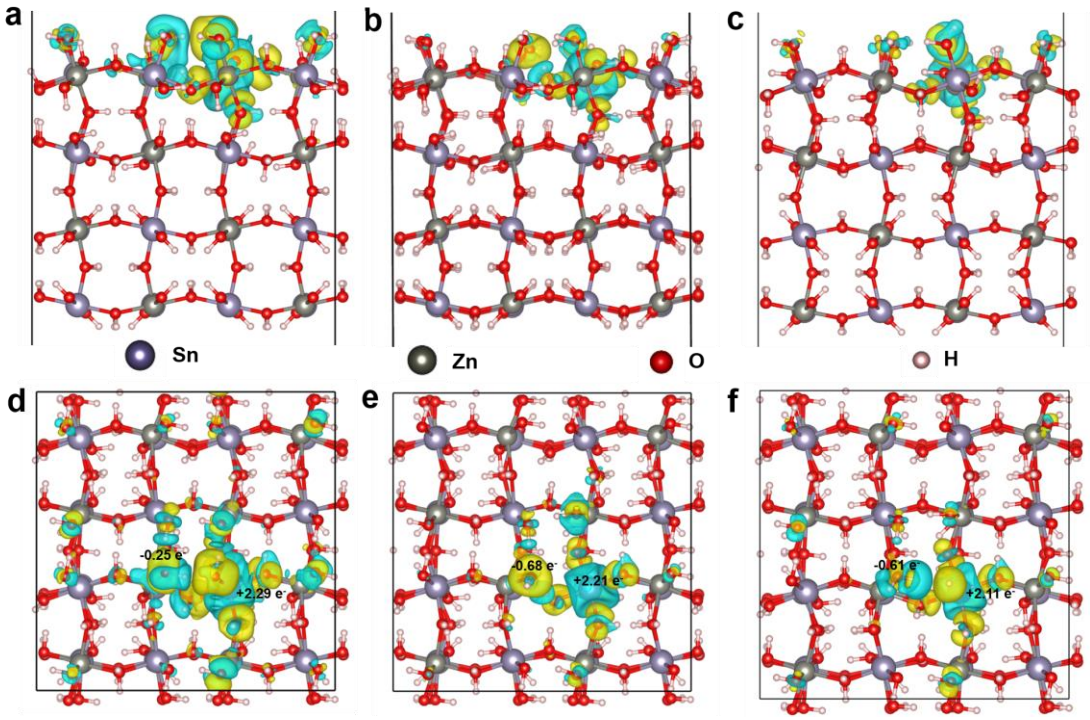


**Fig. S5.** Charge density difference plots of $ZnSn(OH)_6$: (a) and (d) Pristine $ZnSn(OH)_6$ (Sn-OH and Zn-OH sites). (b) and (e) FLPs on $ZnSn(OH)_6$ (Sn-$O_{Vs}$ and Zn-OH sites). (c) and (f) Protonated FLPs on $ZnSn(OH)_6$ (Sn-H and Zn-$OH_2$ sites). Specifically, the Bader charges of Sn-OH and Zn-OH sites were respectively +2.29 e and -0.25 e. After forming the FLPs, the Bader charges of Sn-$O_{Vs}$ and Zn-OH sites were respectively +2.21 e and -0.68 e. After the protonation, the Bader charge of Sn-H and Zn-$OH_2$ sites were +2.11 e and -0.61 e, respectively.

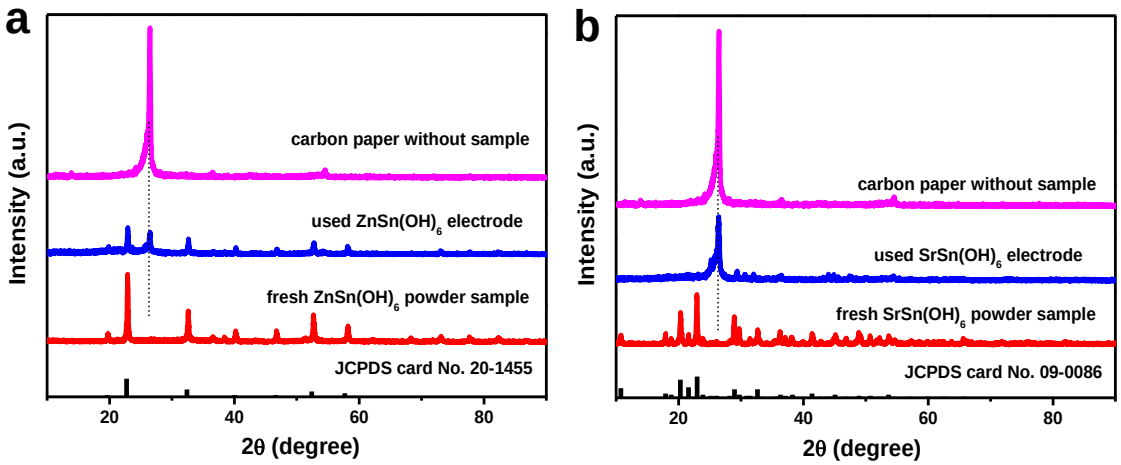


**Fig. S6.** The XRD patterns for $ZnSn(OH)_6$ and $SrSn(OH)_6$ before and after $CO_2$ reduction reaction.

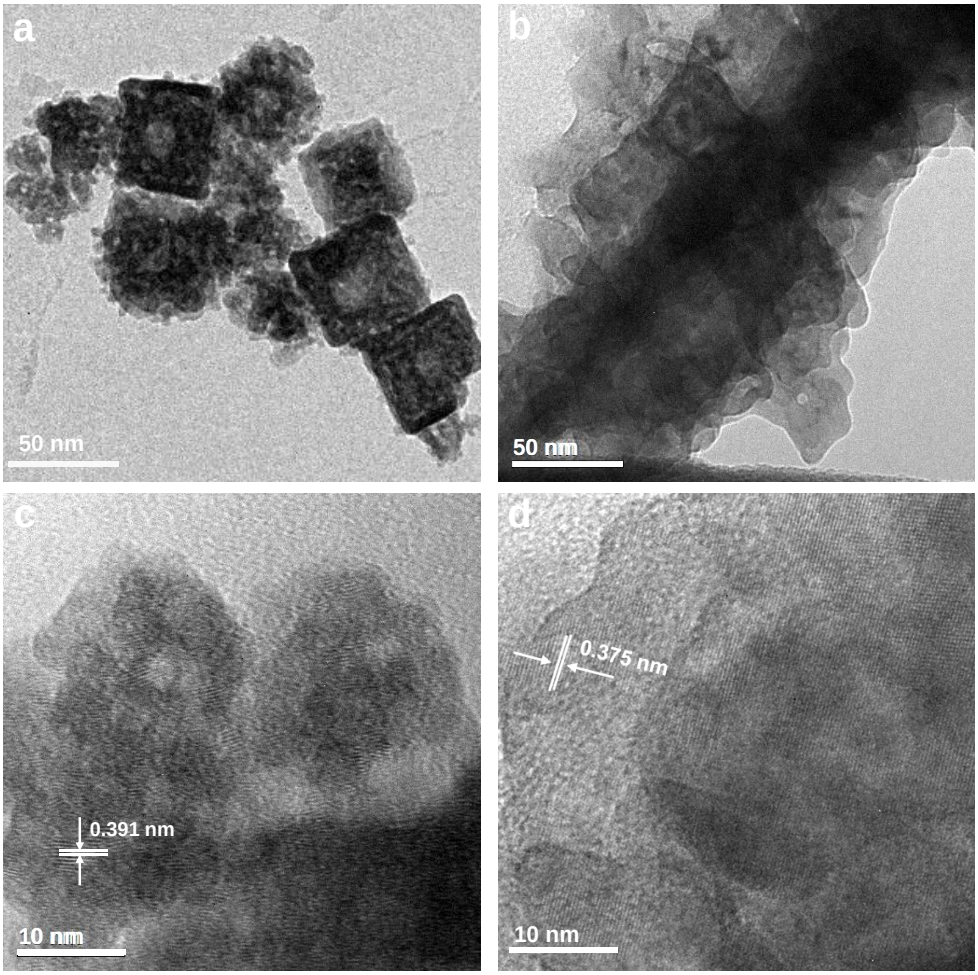


**Fig. S7.** (a) and (c) TEM and HRTEM images for $ZnSn(OH)_6$ after $CO_2$ reduction reaction. (b) and (d) TEM and HRTEM images for $SrSn(OH)_6$ after $CO_2$ reduction reaction.

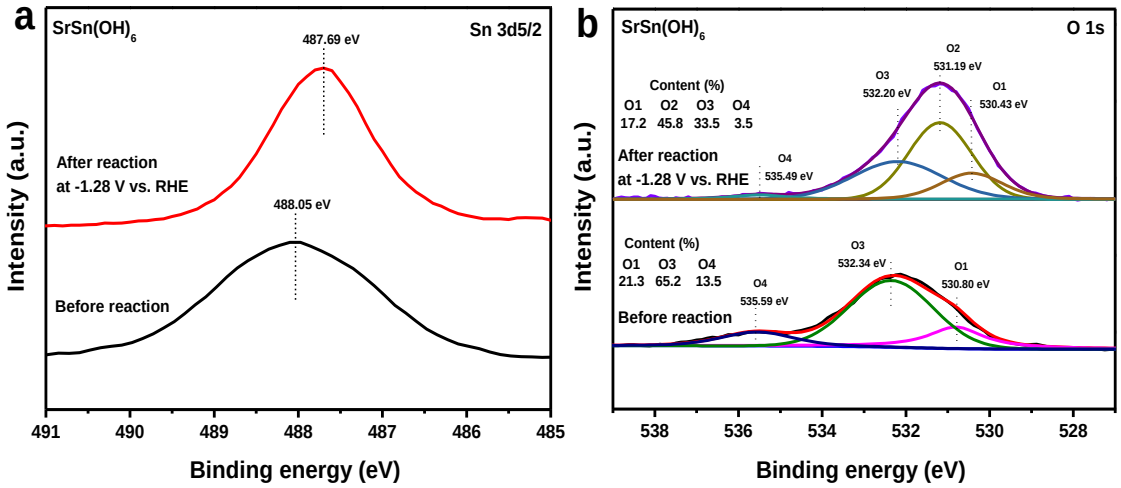


**Fig. S8.** The Sn 3d5/2 (a) and O 1s (b) XPS spectra for $SrSn(OH)_6$ before and after $CO_2$ reduction reaction. Wherein, O1 represents the lattice oxygen or M-OH without vacancies , O2 represents the surface $O_{Vs}$ or defects with low oxygen coordination, O3 and O4 represent the surface-adsorbed -OH, $H_2O$ or $CO_2$ molecules.[1-4]

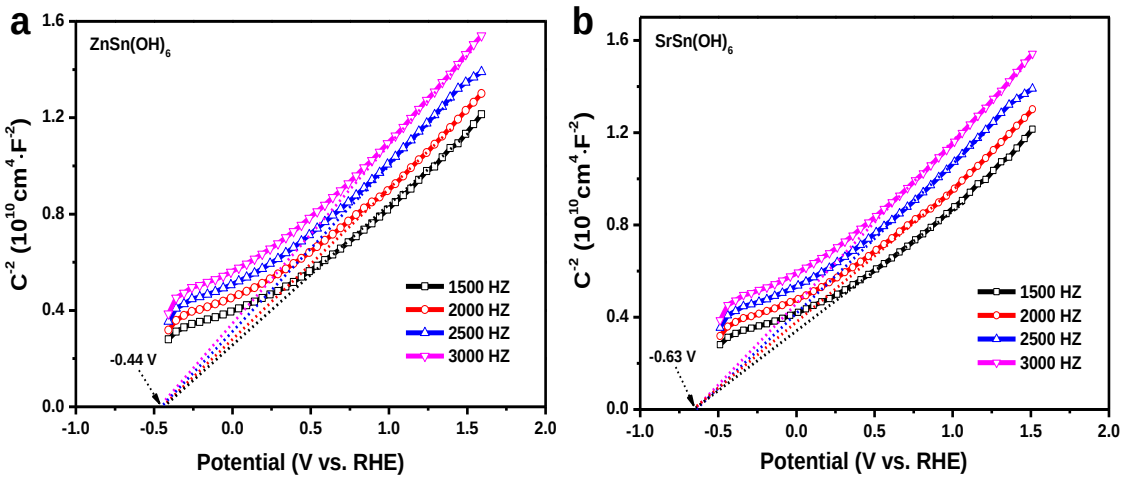


**Fig. S9.** Mott-Schottky plots of $ZnSn(OH)_6$ (a) and $SrSn(OH)_6$ (b) with different frequencies.

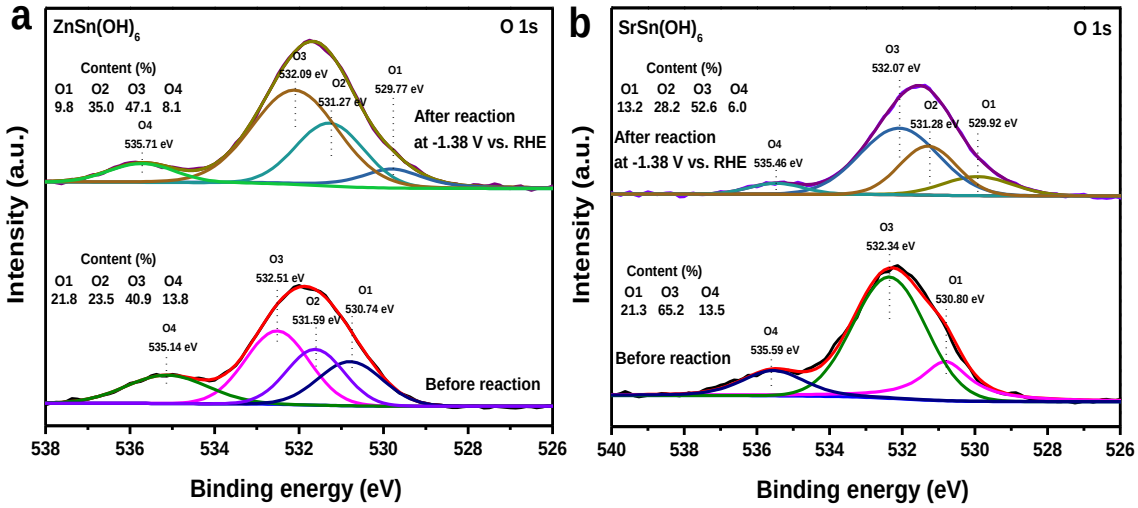


**Fig. S10.** The O 1s XPS spectra for $ZnSn(OH)_6$ (a) and $SrSn(OH)_6$ (b) before and after $CO_2$ reduction reaction. Wherein, O1 represents the lattice oxygen or M-OH without vacancies , O2 represents the surface $O_{Vs}$ or defects with low oxygen coordination, O3 and O4 represent the surface-adsorbed -OH, $H_2O$ or $CO_2$ molecules.[1-4]

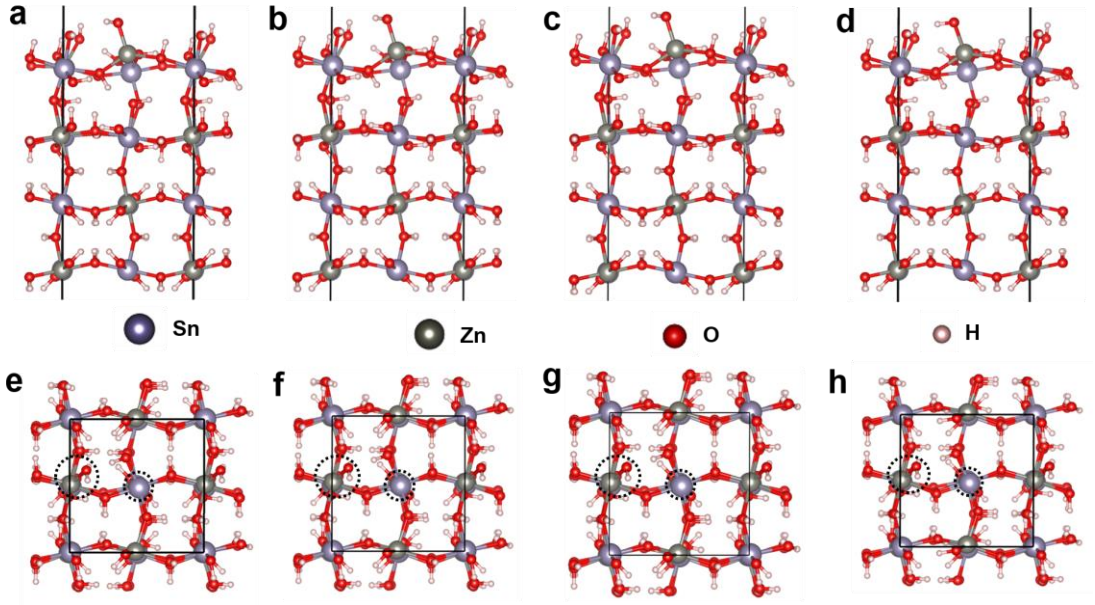


**Fig. S11.** The structure of FLPs (Sn-$O_{Vs}$---Zn-OH) under different vertical electrical field with Ez = 0 V/Å (a and e), -0.1 V/Å (b and f), -0.5 V/Å (c and g) and -1 V/Å (d and h).[5,6]

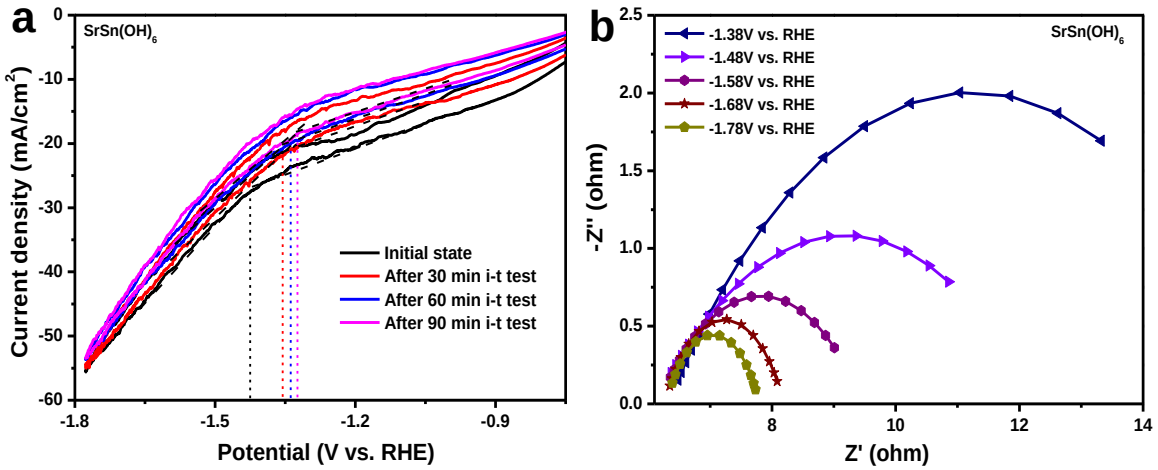


**Fig. S12.** The CV curves ranged from -0.75 V to -1.78 V vs. RHE (a) and EIS spectrum ranged from -1.38 V to -1.78 V vs. RHE (b) of $SrSn(OH)_6$ sample.

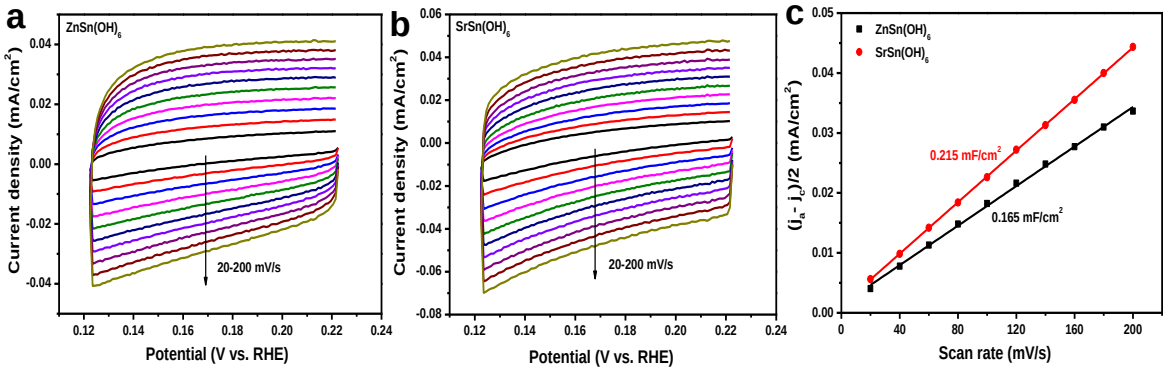


**Fig. S13.** The CV curves of $ZnSn(OH)_6$ (a) and $SrSn(OH)_6$ (b) in $CO_2$ saturated 0.5 M $KHCO_3$ electrolyte at the scan rate from 20 mV/s to 200 mV/s. (c) The linear relationship of the current density versus different scan rates of $ZnSn(OH)_6$ and $SrSn(OH)_6$.

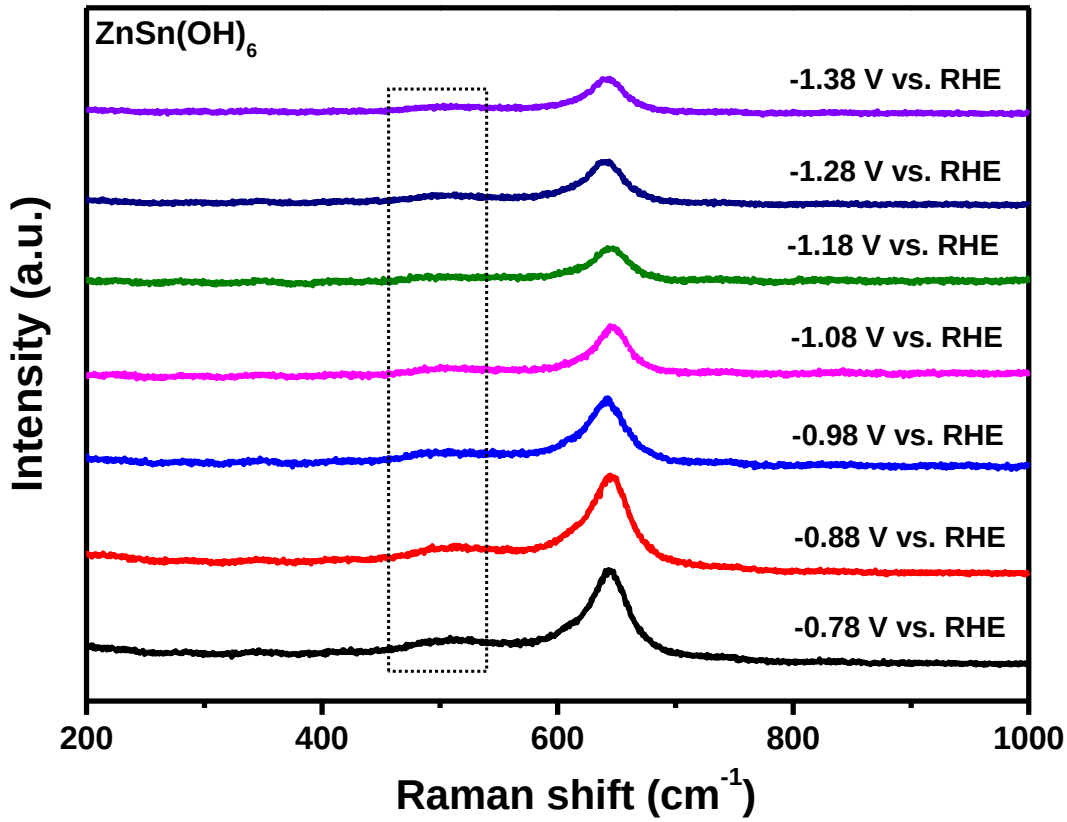


**Fig. S14.** In situ Raman spectrum of $ZnSn(OH)_6$ with different potentials during the catalytic process.

In Raman spectrum, the peak at 645 $cm^{-1}$ was assigned to the anti-symmetric stretching of M-O atoms (M represents metals), which was relevant to the in-plane vibration,[7] and the adjacent broad peak between 460 and 520 $cm^{-1}$ was attributed to the translational vibration of hydroxyl,[8] confirming the presence of M-OH during reaction, further indicating the stable existence of FLPs (Sn-$O_{Vs}$---Zn-OH) during catalytic process.

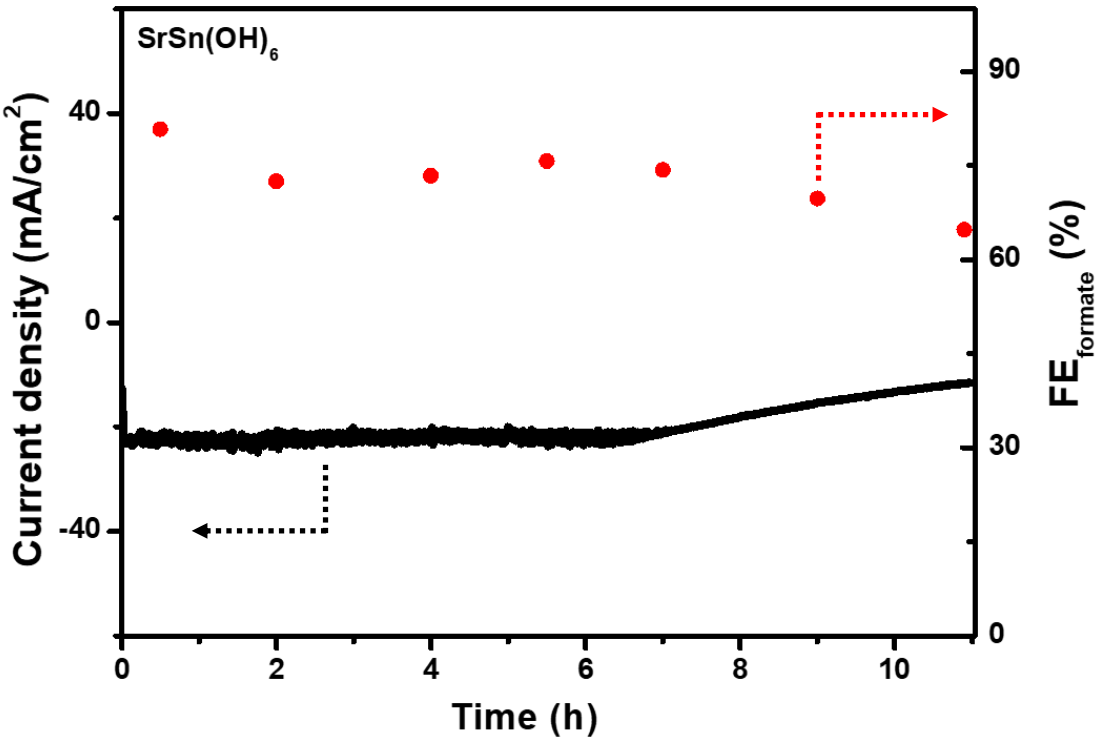


**Fig. S15.** Stability measurement of $SrSn(OH)_6$ by constant potential electrolysis at -1.18 V vs RHE.

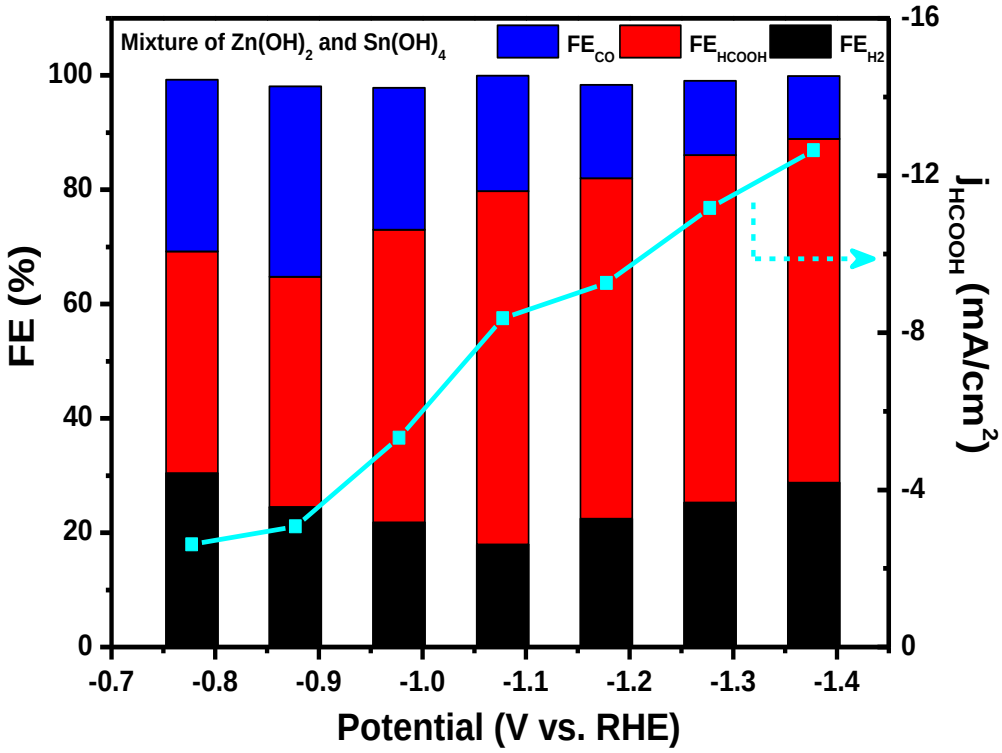


**Fig. S16.** Faradaic efficiencies (FE) and partial current density of formate generation on $Zn(OH)_2$ and $Sn(OH)_4$ mixture at different applied potentials.

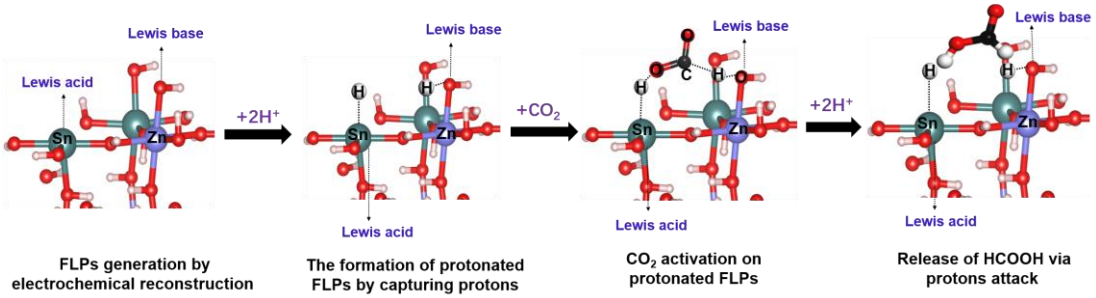


**Fig. S17.** The schematic diagram of $CO_2$ reduction mechanism over FLPs on surface of $ZnSn(OH)_6$.

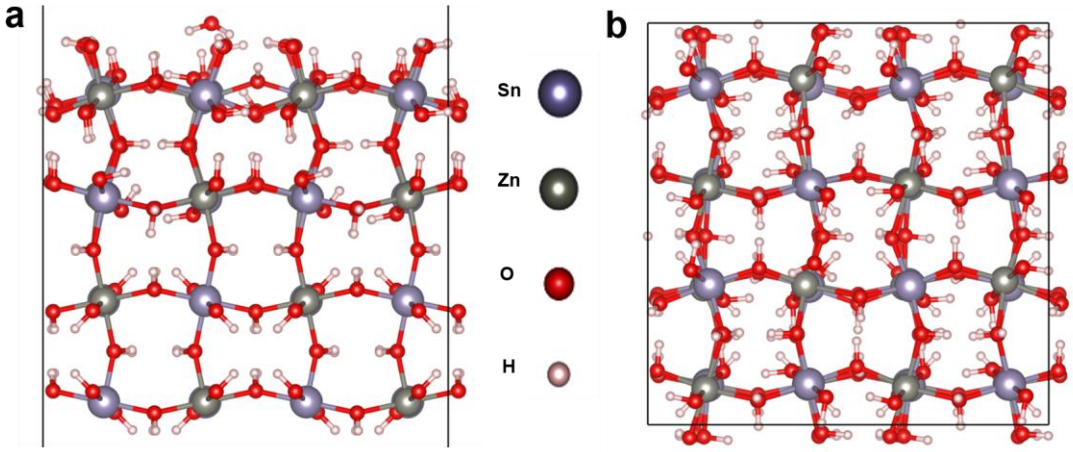


**Fig. S18.** The final optimal active site structure for $ZnSn(OH)_6$.

**Table S1.** The Faraday efficiency (FE) of $CO_2RR$ for $ZnSn(OH)_6$ under different potentials.

| Potential (V *vs.* RHE) | $FE_{H2}$ (%) | $FE_{HCOOH}$ (%) | $FE_{CO}$ (%) | $FE_{CH4}$ (%) |
|---|---|---|---|---|
| -0.78 | 4.12 | 74.18 | 19.24 | 1.24 |
| -0.88 | 6.60 | 80.33 | 11.25 | 1.22 |
| -0.98 | 5.80 | 80.63 | 10.13 | 1.68 |
| -1.08 | 6.69 | 82.28 | 7.66 | 1.63 |
| -1.18 | 9.03 | 82.74 | 5.16 | 1.61 |
| -1.28 | 12.34 | 79.29 | 5.04 | 1.74 |
| -1.38 | 19.91 | 72.32 | 3.56 | 2.02 |

**Table S2.** The Faraday efficiency (FE) of $CO_2RR$ for $SrSn(OH)_6$ for $CO_2RR$ under different potentials.

| Potential (V *vs.* RHE) | $FE_{H2}$ (%) | $FE_{HCOOH}$ (%) | $FE_{CO}$ (%) | $FE_{CH4}$ (%) |
|---|---|---|---|---|
| -0.78 | 11.04 | 57.80 | 26.27 | 1.53 |
| -0.88 | 4.42 | 66.60 | 23.56 | 1.59 |
| -0.98 | 4.11 | 74.95 | 16.99 | 1.82 |
| -1.08 | 4.20 | 80.43 | 13.74 | 0.99 |
| -1.18 | 9.94 | 80.69 | 6.63 | 0.89 |
| -1.28 | 15.07 | 76.23 | 5.53 | 1.18 |
| -1.38 | 32.55 | 57.86 | 5.81 | 1.38 |

**Table S3.** The Faraday efficiency (FE) of $CO_2RR$ for the physical mixture of $Zn(OH)_2$ and $Sn(OH)_4$ under different potentials.

| Potential (V *vs.* RHE) | $FE_{H2}$ (%) | $FE_{HCOOH}$ (%) | $FE_{CO}$ (%) |
|---|---|---|---|
| -0.78 | 30.42 | 38.82 | 30.02 |
| -0.88 | 24.51 | 40.26 | 33.35 |
| -0.98 | 21.83 | 51.20 | 24.82 |
| -1.08 | 17.94 | 61.82 | 20.20 |
| -1.18 | 22.44 | 59.56 | 16.35 |
| -1.28 | 25.30 | 60.79 | 12.97 |
| -1.38 | 28.75 | 60.15 | 10.99 |

**References**


1. H. Yan, Q. Shen, Y. Sun, S. Zhao, R. Lu, M. Gong, Y. Liu, X. Zhou, X. Jin, X. Feng, X. Chen, D. Chen, C. Yang, *ACS Catal.*, 2021, **11**, 6371-6383.
2. Y.-F. Jiang, N. Jiang, K. Liang, C.-Z. Yuan, X.-X. Fang, A.-W. Xu, *J. Mater. Chem. A*, 2019, **7**, 7932-7938.
3. P. D. Schulze, S. L. Shaffer, R. L. Hance, D. L. Utley, *J. Vac. Sci. Technol. A*, 1983, **1**, 97-99.
4. M. K. Rajumon, M. S. Hegde, C. N. R. Rao, *Catal. Lett.*, 1988, **1**, 351-360.
5. Y. Li, S. X. Yang and J. B. Li, *J. Phys. Chem. C*, 2016, **118**, 23970-23976.
6. P. J. Feibelman, *Phys. Rev. B*, 2001, **64**, 125403.
7. Y. Cao, Q. Ye, F. Wang, X. Fan, L. Hu, F. Wang, T. Zhai, H. Li, *Adv. Func. Mater.*, 2020, **30**, 2003733.
8. J. Hao, L. Yuan, Y. Zhu, M. Jaroniec, S.-Z. Qiao, *Adv. Mater.*, 2022, **34**, 2206963.